The Co-Mn (Cobalt-Manganese) System

By K. Ishida and T. Nishizawa
Tôhoku University

Equilibrium Diagram

The assessed Co-Mn phase diagram (Fig. 1) is based primarily on the investigations of [57Hel], [71Tsi], and [82Has]. The phases included in Fig. 1 are: (1) the liquid, L; (2) the fcc terminal solid solutions, (αCo) and (γMn); (3) the cph solid solution, (εCo); (4) the Mn-rich bcc solid solution, (δMn); (5) the solid solution, (βMn); (6) complex cubic (αMn) below 710 °C; and (7) the σ phase, formed at about 50 at.% Mn below 545 °C. Special points of Fig. 1 are summarized in Table 1.

Liquidus and Solidus

The liquidus and solidus as determined by thermal analysis are summarized in Table 2. The experimental data on the Co-rich side of [32Has], [37Has], and [49Sch] and on Mn-rich side of [49Sch], [57Hel], and [71Tsi] generally agree well, as shown in Fig. 2. [57Hel] reported that the peritectic reaction L + (αCo) ↔ (βMn) occurs at 1161 °C, which is consistent with the 1160 °C determined by [71Tsi]. The liquidus and solidus continue to fall to a minimum at about 63 at.% Mn and 1160 °C [57Hel]. The peritectic reaction L + (δMn) ↔ (βMn) occurs at 1182 °C, according to [57Hel], or at 1190 °C, according to [71Tsi].

Solid Phase Equilibria

The experimental data on the solid phase equilibria concerned with (αCo), σ, (αMn), (βMn), (γMn), and (δMn) are summarized in Table 3 and Fig. 3. The (αCo)/(βMn) equilibrium was investigated by thermal analysis and metallographic examination [57Hel, 71Tsi] and by electron probe microanalysis [82Has]. The agreement of these results is fairly good. The phase equilibria between (βMn), (γMn), and (δMn) in the Mn-rich region were studied by [57Hel] and [71Tsi] with thermal analysis. These experiments confirmed the peritectoid reaction (βMn) + (δMn) ↔ (γMn) at about 1150 °C, which refuted the continuous solid solution of (γMn) and (αCo) proposed in the previous diagram by [Hansen]. [71Tsi] also determined the phase boundary below 600 °C by metallographic study on heavily deformed specimens. They found that σ is formed by peritectoid reaction from (αCo) and (βMn) below 545 °C at 50 at.% Mn.

Table 1 Special Points of the Assessed Co-Mn Phase Diagram

Reaction	Compositions of the respective phases, at.% Mn			Temperature, °C	Reaction type	Reference
L ↔ αCo		0		1495	Melting point	[83Nis1]
αCo ↔ εCo		0		422	Allotropic	[Massalski]
L + (αCo) ↔ (βMn)	~61.9	~57.5	61.7	1161	Peritectic	[57Hel]
	63.5	59.5	62.5	1160	Peritectic	[72Tsi]
	60.5	58.5	60.3	1161	Peritectic	[82Has]
	62.0	59.0	61.8	1161		(a)
(αCo) + (βMn) ↔ σ	~49	~52	~50	545	Peritectoid	[72Tsi]
	~48	~52	~50	545		(a)
L ↔ (βMn)		63 to 64		1160	Congruent	[57Hel]
		63.5		1160		(a)
L + (δMn) ↔ (βMn)	88.8	91.0	90.0	1182	Peritectic	[57Hel]
	89.5	91.5	90.5	1190	Peritectic	[71Tsi]
	88.1	90.6	89.5	1186	Peritectic	[82Has]
	89.0	91.0	89.5	1185		(a)
(βMn) + (δMn) ↔ (γMn)	~95.2	~96.0	~95.7	~1148	Peritectoid	[57Hel]
	93.5	96.0	95.0	1153	Peritectoid	[72Tsi]
	94.5	95.8	95.6	1151	Peritectoid	[82Has]
	94.5	96.0	95.7	1150		(a)
L ↔ δMn		100		1246	Melting point	[Melt]
δMn ↔ γMn		100		1143	Allotropic	[Massalski]
γMn ↔ βMn		100		1079	Allotropic	[Massalski]
βMn ↔ αMn		100		710	Allotropic	[Massalski]

(a) From the assessed phase diagram.

Co-Mn

The assessed phase diagram shows the miscibility gap in (αCo) along the Curie temperature, which is based on thermodynamic calculations by [82Has]. This magnetically-induced phase separation was also examined by high-temperature X-ray diffraction [81Ind2].

Metastable Phases

(γMn) and (γ'Mn)

(γMn) cannot be retained by quenching pure Mn, but transforms to fct γ' [Pearson1, 58Wei]. [49Sch] reported

Fig. 1 Assessed Co-Mn Phase Diagram

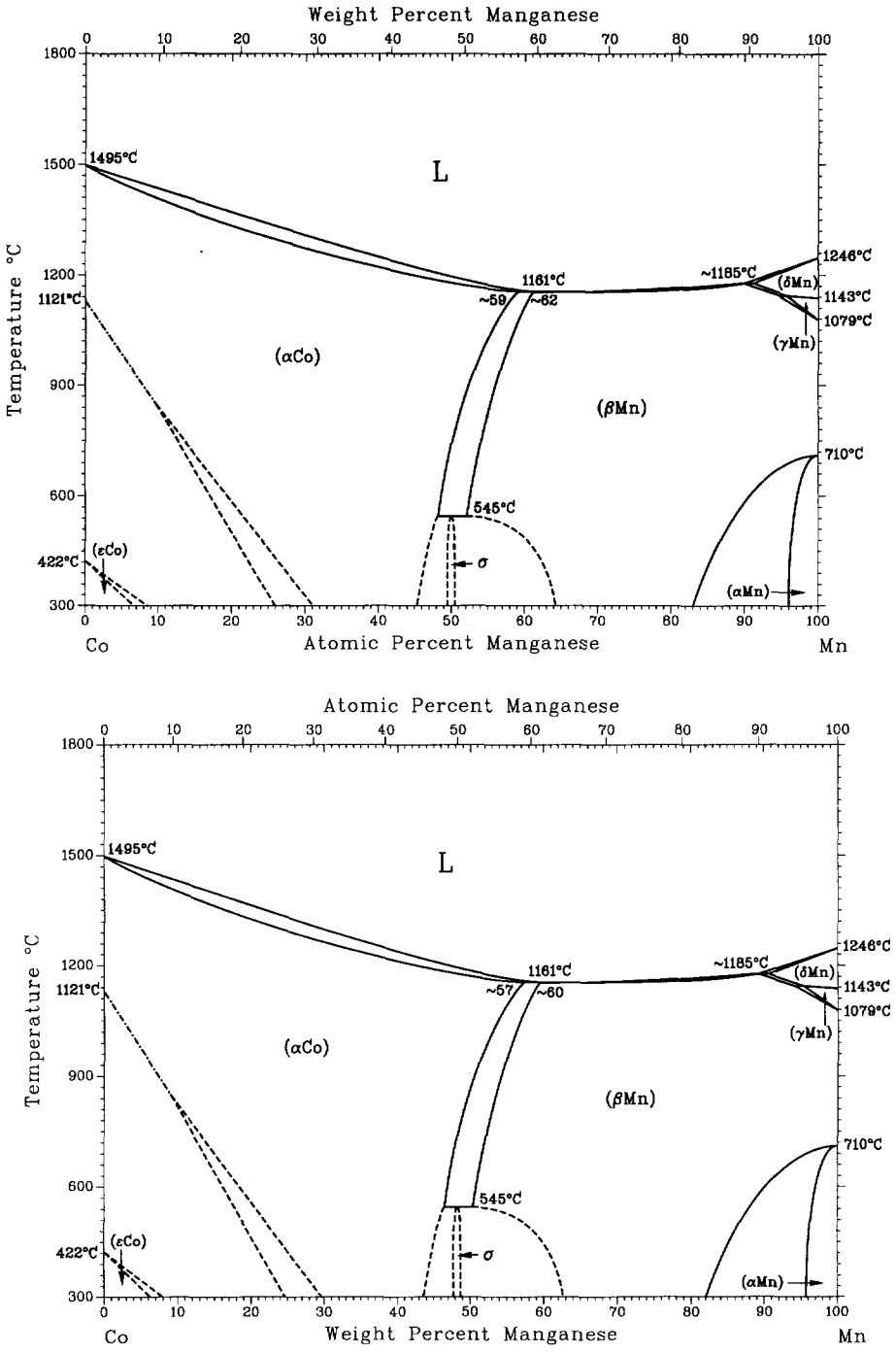

K. Ishida and T. Nishizawa, 1990.

that the (γ'Mn) single phase is formed by quenching from the high-temperature solid field of (γMn). (γ'Mn) is also formed in the composition range of 91 to 100 at.% Mn by splat quenching from the melt [75Gud]. Metastable (γMn) was found in specimens obtained by rapid solidification in the range of 60 to 88 at.% Mn [75Gud].

(αCo) ↔ (εCo) Martensitic Transformation

The (αCo) ↔ (εCo) martensitic transformation temperatures were examined by thermal analysis [32Has, 37Has, 71Tsi], dilatometric measurements [70Mas], magnetic analysis [37Has, 70Mas], and electrical resistivity [70Mas, 71Sha]. The experimental data are given in Table 4 and Fig. 4. Both the transformation temperatures on heating (A_s) and cooling (M_s) decrease with increasing Mn content.

Crystal Structure and Lattice Parameters

The crystal structure and lattice parameters of stable and metastable Co-Mn phases are summarized in Tables 5 and 6, respectively. The lattice parameters of the stable (αCo) phase reported by [32Has], [33Kos], [49Sch], and [Pearson1] are shown in Fig. 5, together with the data on metastable (αCo) produced by splat quenching from a liquid state [75Gud]; the data of [49Sch] above 60 at.% Mn were omitted, because the presence of the fcc phase in this composition range is doubtful. [72Wei] proposed that (γMn) has three distinct states—antiferromagnetic γ_1, paramagnetic γ_2, and ferromagnetic γ_3, with lattice parameters of 0.369 ± 0.01, 0.359 ± 0.03, and 0.382 ± 0.02 nm, respectively. The lattice parameters of metastable (γ'Mn) and (εCo) were measured by [49Sch], [75Gud], and [33Kos].

Thermodynamics

[79Ben] measured the specific heat of Co-rich (αCo) below 1400 K. Anomalous behavior of the heat capacities was observed in the vicinity of the Curie temperatures, but the Curie peaks diminished rapidly with increasing Mn content.

The low-temperature (1 to 4 K) specific heats of Co-rich (εCo) were studied by [80Gre] and were described by the equation $C = \gamma T + \beta T^3 + \kappa T^{-2}$. The values of the

Table 2 Co-Mn Liquidus and Solidus Data from Thermal Analysis

Composition, at.% Mn	Temperature, °C Liquidus	Solidus	Composition, at.% Mn	Temperature, °C Liquidus	Solidus
From [32Has]			**From [57Hel]**		
5.27	1481	1461	53.9	1181	1170
10.67	1450	1422	56.44	1173	1163
15.89	1410	1376	58.3	1167	1160
21.16	1370	1339	61.9	1161	1160
31.63	1291	1259	63.64	1160.5	1160.5
42.7	1235	1212	70.3	1166	1165
53.0	1183	1167	75.2	1169	1168
From [37Has]			80.4	1174	1172
5.3	1480	1461	83.8	1177	1175
10.7	1453	1422	86.25	1180.5	1178
15.9	1413	1379	89.8	1187.5	1180
21.1	1370	1334	90.73	1193	1182
31.5	1293	1255	92.16	1201.5	1189
From [49Sch](a, b)			95.15	1216	1210
10.6	1446	1420	96.14	1222	1216
21.1	1376	1340	98.96	1237.5	1235
31.5	1304	1270	**From [71Tsi]**(b)		
41.7	1244	1216	50.0	1212	1180
51.7	1198	1176	52.1	1203	1175
56.7	1176	1150	56.8	1183	1166
61.7	1168	1150	61.5	1170	1160
71.4	1170	1152	66.5	1154	1154
81.1	1184	1160	71.5	1162	1158
88.7	1184	1162	77.4	1171	1163
90.6	1200	1174	90.0	1193	1188
94.4	1220	1200	92.1	1197	1197
96.3	1230	1210	95.1	1126	1214
98.1	1244	1226	97.1	1237	1226

(a)Unpublished work by Grube and Fischer cited in [49Sch]. (b)Data read from the figure.

Fig. 2 Liquidus and Solidus in the Co-Mn System

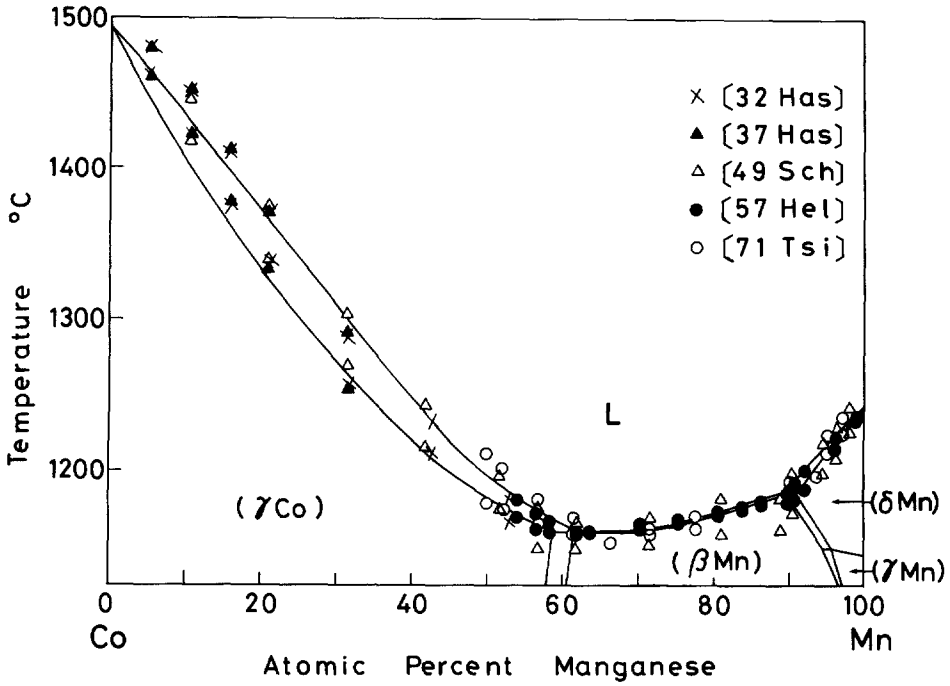

K.Ishida and T. Nishizawa, 1990.

Fig. 3 Solid Phase Equilibria in the Co-Mn System

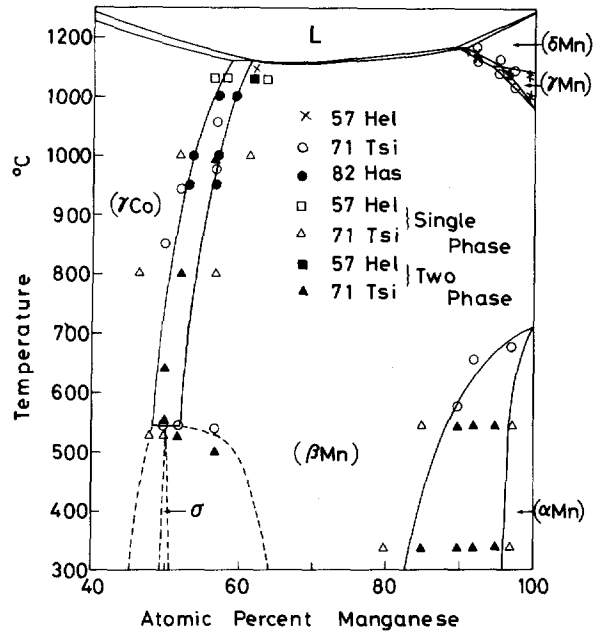

The (δMn) + (γMn) two-phase region is too narrow to draw.

K. Ishida and T. Nishizawa, 1990.

Fig. 4 Experimental Data on the Martensitic Transformation Temperatures

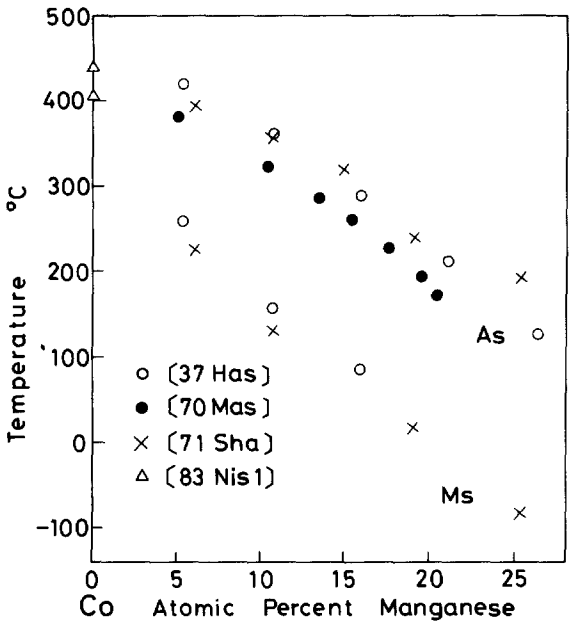

K. Ishida and T. Nishizawa, 1990.

electronic, lattice and hyperfine specific heat coefficients γ, β, and κ are given in Table 7. The heat capacities of pure αMn and βMn at low temperatures were measured by [45Sho] and [55Boo]. The magnetic specific heat of αMn was estimated from the total heat capacity by [57Tau].

The activities of Mn in the liquid state were determined by emf measurement, using a ThO_2-Y_2O_3 electrolyte at 1760 K [82Jac], and by the isobaric method using an alumina capsule in the temperature range of 1743 to 1893 K [82Muk]. [67Ere] and [82Ven] measured the activities of Mn in the solid phases with emf at 1073 and 973 to 1348 K, respectively. Both the liquid and solid solutions were found to exhibit large negative deviations from ideal solution behavior.

The lattice stability parameters were evaluated for Co and Mn by [73Kau], [78Kau], [82Has], and [87Gui] and by [58Wei], [78Kau], [83Cha], and [86Hil], respectively. The interaction parameters were reported for the liquid by [78Kau], [82Has], and [82Jac]; for (βMn), (γMn), and (δMn) by [78Kau] and [82Has]; and for (αMn) and (εCo) by [78Kau]. Calculations of the Co-Mn phase diagram were carried out by [78Kau] and [82Has] on the basis of the thermodynamic parameters given in Tables 8 and 9. According to [82Has], the Gibbs energies of the solution phases may be represented by:

$$G = [G^0_{Co}]^P(1-x) + [G^0_{Mn}]^P x + RT[x \ln x + (1-x)\ln(1-x)] + [\Omega_{CoMn}]^P x(1-x) + \Delta G^{mag}$$

where $[G^0]^P$ and $[\Omega_{CoMn}]^P$ are the Gibbs energies of the pure components and the interaction parameter in the paramagnetic state, respectively. ΔG^{mag} is the magnetic term of the Gibbs energy, which is described in the form of [83Nis2] (essentially equivalent to that of [81Ind1]), and X is the mole fraction of Mn.

The present calculation is based on the thermodynamic parameters of [82Has], with the lattice stability

Table 3 Experimental Data on Solid Phase Equilibria in the Co-Mn System

Temperature, °C	Composition, at.% Mn (αCo)	(αMn)	(βMn)	(γMn)	(δMn)
From [57Hel](a)					
1150	...	...	...	61.9	...
1178	...	...	90.73	...	...
1181	...	...	...	...	90.73
1168	...	...	92.16	...	...
1173	...	...	...	...	92.16
1151	...	...	95.15	...	95.15
1137	...	...	96.14	...	...
1140	...	...	...	96.14	...
1145	...	...	...	96.14	96.14
1102.5	...	...	98.96	...	...
1105.5	...	...	...	98.96	...
1137.5	...	...	...	98.96	...
1140	...	...	...	...	98.96
From [71Tsi](a, b)					
851	50.0	...	...	...	...
946	52.1	...	...	...	...
542	...	...	56.8	...	...
977	...	...	56.8	...	...
1054	56.8	...	...	...	...
579	...	...	90.0	...	...
657	...	...	92.1	...	...
1163	...	...	92.1	...	...
1186	...	...	...	...	92.1
1140	...	...	...	95.1	...
1165	...	...	...	...	95.1
679	...	...	97.1	...	...
1117	...	...	97.1	97.1	...
1149(c)	...	...	...	97.1	97.1
800(c)	49.5	...	52.5	...	...
300	...	97.0	84.0	...	...
From [82Has](d)					
950	53.2	...	56.8	...	...
1000	53.7	...	57.0	...	...
1100	57.0	...	59.3	...	...

(a)Thermal analysis. (b)Data read from the figure. (c)Metallographic examination. (d)EPMA.

parameters for Mn altered to those of [83Cha]. The calculated result is shown in Fig. 6, together with that of [78Kau]. Figures 7 and 8 show the computed values for activities of Mn and Co at 750 and 1570 °C respectively, in comparison with the experimental data [67Ere, 82Muk, 82Ven].

Magnetism

(αCo) and (εCo) are ferromagnetic; the change in Curie temperature with Mn content was investigated by [32Has], [37Has], [57Cra], [70Mas], [70Mat], [71Tsi], and [85Men]. The magnetic moments of (αCo) and (εCo) were also determined by [57Cra]. The transition from ferromagnetic to antiferromagnetic in (αCo) occurs near 30 at.% Mn at room temperature. The magnetic properties and the transition temperatures in the range 30 to 60 at.% Mn were studied mainly by neutron diffraction experiments [70Mat, 72Ada, 80Rhi, 85Men]. The magnetic properties of the four pure Mn allotropic modifications—αMn, βMn, γMn, and δMn—were summarized by [58Wei]. The Néel temperature, T_N, of pure αMn is about 95 K [56Kas], and its magnetic structure was determined by [53Shu], [56Kas], [57Tau], and [70Yam]. Using electrical resistivity measurements, [76Wil] determined the change in T_N with addition of Co to αMn to be about 26 K for 1 at.% Co.

Table 4 Martensitic Transformation Temperatures in the Co-Mn Alloys

Reference	Method	Composition, at.% Mn	Transformation temperature, °C As		Ms	$\alpha \leftrightarrow \varepsilon$
[32Has]	Thermal analysis	5.27	...		...	259
		10.67	...		...	158
[37Has]	...	5.3	420(a)	421(b)	259(a, b)	...
		10.7	364(a)	360(b)	157(a, b)	...
		15.9	290(a)	289(b)	85(a, b)	...
		21.1	214(a)		...	...
		26.3	128(a)			
[70Mas](c)	Dilatometry, magnetic measurements, electrical resistivity	5.0	381		...	...
		10.3	324		...	...
		13.4	288		...	...
		15.4	261		...	...
		17.5	228		...	...
		19.5	194		...	...
		20.4	173		...	...
[71Sha](c)	Electrical resistivity	6.04	395		225	...
		10.7	358		133	...
		14.9	320		...	...
		19.1	242		18	...
		25.4	195		-83	...
[71Tsi](c)	Thermal analysis	15.3	...		...	182
		20.6	...		...	88
[83Nis1]	...	0	(~440)		(~405)	...

(a)Dilatometry. (b)Magnetic measurements. (c)Data read from the figure.

Table 5 Co-Mn Crystal Structure Data

Phase	Composition, at.% Mn	Pearson symbol	Space group	Strukturbericht designation	Prototype	Reference
(αCo)	0 to 60	*cF*4	$Fm\bar{3}m$	*A*1	Cu	[83Nis1]
(εCo)	0 to ~20	*hP*2	$P6_3/mmc$	*A*3	Mg	[83Nis1]
σ	~ 50	*tP*30	$P4_2/mnm$	$D8_b$	σCrFe	[71Tsi]
(αMn)	97 to 100	*cI*58	$I\bar{4}3m$	*A*12	αMn	[Pearson1]
(βMn)	51 to 100	*cP*20	$P4_132$	*A*13	βMn	[Pearson1]
(γMn)	95 to 100	*cF*4	$Fm\bar{3}m$	*A*1	Cu	[Pearson1]
(δMn)	91 to 100	*cI*2	$Im\bar{3}m$	*A*2	W	[Pearson1]
Metastable phases						
(γMn)(a)	60 to 88	*cF*4	$Fm\bar{3}m$	*A*1	Cu	[75Gud]
(γ'Mn)	95 to 100(b)	*tI*2	*I*4/*mmm*	*A*6	In	[49Sch]
	91 to 100(a)	*tI*2	*I*4/*mmm*	*A*6	In	[75Gud]

(a)Splat quenched from the liquid. (b)Rapidly quenched from the high-temperature solid field.

Table 6 Co-Mn Lattice Parameter Data

Phase	Composition, at.% Mn	Lattice parameters, nm a	c	Reference
αCo	0	0.35446	...	[83Nis1]
(αCo)	31.6	0.3568	...	[32Has]
	42.7	0.3573	...	[32Has]
	52.9	0.3578	...	[32Has]
(αCo)	31.5	0.3561	...	[33Kos]
	39.7	0.3584	...	[33Kos]
	46.7	0.3596	...	[33Kos]
(αCo)(a)	10.6	0.3554	...	[49Sch]
	21.1	0.3563	...	[49Sch]
	31.4	0.3569	...	[49Sch]
	36.6	0.3576	...	[49Sch]
	41.7	0.3580	...	[49Sch]
	46.7	0.3595	...	[49Sch]
	51.8	0.3605	...	[49Sch]
	56.7	0.3626	...	[49Sch]
(αCo)	7.84	0.35585	...	[Pearson1]
	9.42	0.35604	...	[Pearson1]
	20.70	0.35675	...	[Pearson1]
	22.92	0.35690	...	[Pearson1]
	28.15	0.35736	...	[Pearson1]
	31.73	0.35775	...	[Pearson1]
	46.84	0.36059	...	[Pearson1]
	48.86	0.36122	...	[Pearson1]
	52.22	0.36185	...	[Pearson1]
	53.67	0.36324	...	[Pearson1]
	54.0	0.36248	...	[Pearson1]
(αCo)	48.0	0.3606	...	[73Ada]
εCo	0	0.25071	0.40695	[83Nis1]
(εCo)	4.3	0.2506	0.4074	[33Kos]
	8.0	0.2510	0.4076	[33Kos]
	15.9	0.2515	0.4085	[33Kos]
	21.1	0.2516	0.4086	[33Kos]
(βMn)	56.92	0.6282	...	[Pearson1]
	58.79	0.6283	...	[Pearson1]
	60.47	0.6288	...	[Pearson1]
	60.72	0.6289	...	[Pearson1]
	61.40	0.6291	...	[Pearson1]
	68.47	0.6310	...	[Pearson1]
	68.74	0.6310	...	[Pearson1]
	72.81	0.6314	...	[Pearson1]
	74.56	0.6317	...	[Pearson1]
	79.64	0.6321	...	[Pearson1]
	80.62	0.6320	...	[Pearson1]
	86.72	0.6324	...	[Pearson1]
	86.95	0.6323	...	[Pearson1]
	88.89	0.6319	...	[Pearson1]
	88.95	0.6328	...	[Pearson1]
	89.48	0.6321	...	[Pearson1]
	90.57	0.6322	...	[Pearson1]
	95.71	0.6324	...	[Pearson1]
	96.04	0.6319	...	[Pearson1]
(αMn)	100	0.89139	...	[Pearson2]
(βMn)	100	0.63145	...	[Pearson2]
(γMn)(b)	100	0.38624	...	[Pearson2]

(a) Rapidly quenched from the high-temperature solid field. **(b)** At 1095 °C. **(c)** At 1134 °C. **(d)** Splat quenched from the liquid. Data read from the figure.

(continued)

Table 6 Co-Mn Lattice Parameter Data (continued)

Phase	Composition, at.%Mn	Lattice parameters, nm a	c	Reference
(δMn)(c)	100	0.30806	...	[Pearson2]
Metastable phases				
(αCo)(a)	61.7	0.3644	...	[49Sch]
	66.6	0.3655	...	[49Sch]
	71.4	0.3670	...	[49Sch]
	76.3	0.3679	...	[49Sch]
	81.2	0.3691	...	[49Sch]
	85.8	0.3698	...	[49Sch]
	88.7	0.3705	...	[49Sch]
	90.6	0.3716	...	[49Sch]
(γMn)(d)	58.7	0.3617	...	[75Gud]
	62.7	0.3625	...	[75Gud]
	64.1	0.3629	...	[75Gud]
	80.6	0.3674	...	[75Gud]
	88.2	0.3684	...	[75Gud]
(γ'Mn)	92.5	0.3724	0.370	[49Sch]
	94.4	0.3737	0.3660	[49Sch]
	95.3	0.3748	0.3642	[49Sch]
	96.2	0.3755	0.3632	[49Sch]
(γ'Mn)	90.6	0.3726	0.3674	[75Gud]
	95.3	0.3748	0.3628	[75Gud]
(γ'Mn)	100	0.3782	0.3547	[Pearson2]

(a)Rapidly quenched from the high-temperature solid field. (b)At 1095 °C. (c)At 1134 °C. (d)Splat quenched from the liquid. Data read from the figure.

Table 7 Parameters for Low-Temperature Specific Heat of (εCo) Alloys
$C = \gamma T + \beta T^3 + \kappa T^{-2}$

Composition, at.% Mn	Coefficients γ μJ/mol · K²	β μJ/mol · K⁴	κ μJ · K/mol
1	4527	20.1	4622
2	4725	20.0	4506
3	5192	18.9	4217
5	6311	16.7	3758
7	7258	15.4	3403

From [80Gre].

The experimental results on the magnetic properties of the Co-Mn alloys are summarized in Table 10. On the basis of these data, the magnetic phase diagram was constructed as shown in Fig. 9.

Fig. 5 Lattice Parameters of (αCo)

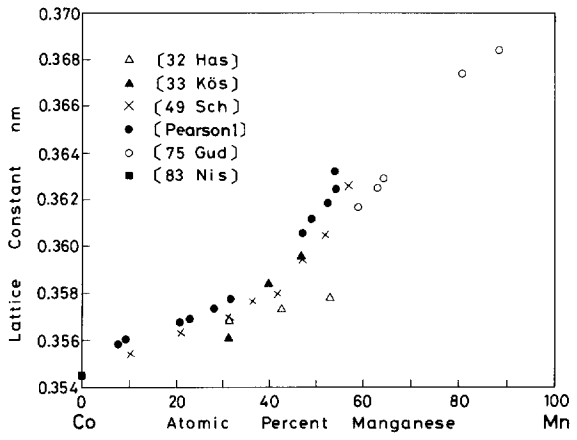

K. Ishida and T. Nishizawa, 1990.

Cited References

32Has: U. Hashimoto, "Co-Mn Alloys," *Kinzoku-no-Kenkyu, 9*, 64-65 (1932) in Japanese. (Equi Diagram, Meta Phases, Crys Structure, Magnetism; Experimental)

33Kos: W. Köster and W. Schmidt, "On the Iron-Cobalt-Manganese System," *Arch. Eisenhüttenwes., 2*, 121-126 (1933) in German. (Crys Structure; Experimental)

37Has: U. Hashimoto, "Relation Between the Allotropic Transformation of Cobalt and Some Additional Elements," *J. Jpn. Inst. Met., 1*, 177-190 (1937) in Japanese. (Equi Diagram, Meta Phases, Magnetism; Experimental)

45Sho: C.H. Shomate, "Low Temperature Specific Heats of α-Manganese and γ-Manganese," *J. Chem. Phys., 13*, 326-332 (1945). (Thermo; Experimental)

49Sch: A. Schneider and W. Wunderlich, "γ-Phase in the Co-Mn System," *Z. Metallkd., 40*, 260-263 (1949) in German.

(Equi Diagram, Meta Phases, Crys Structure; Experimental)

53Shu: C.G. Shull and M.K. Wilkinson, "Neutron Diffraction Studies of Various Transition Elements," *Rev. Mod. Phys.*, *25*, 100-109 (1953). (Magnetism; Experimental)

55Boo: G.L. Booth, F.E. Hoare, and B.T. Murphy, "The Low Temperatures (11-20 K) Specific Heat of α and β Man-

Fig. 6 Calculated Co-Mn Phase Diagram

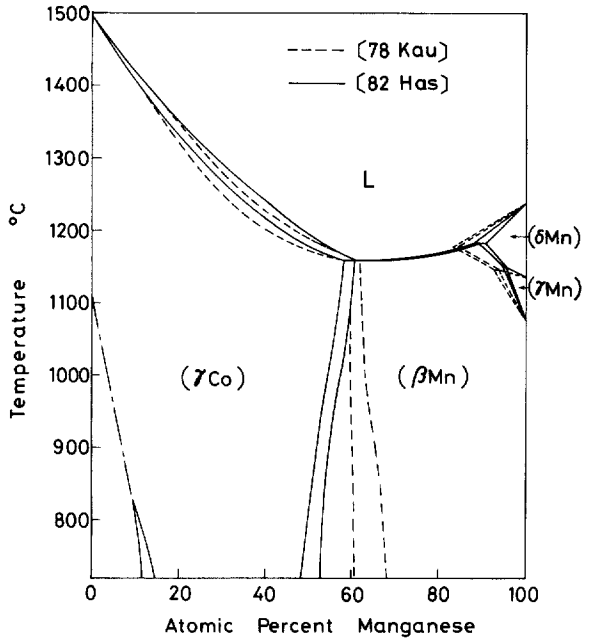

K. Ishida and T. Nishizawa, 1990.

Fig. 7 Calculated Activities of Mn and Co at 750 °C with Experimental Data

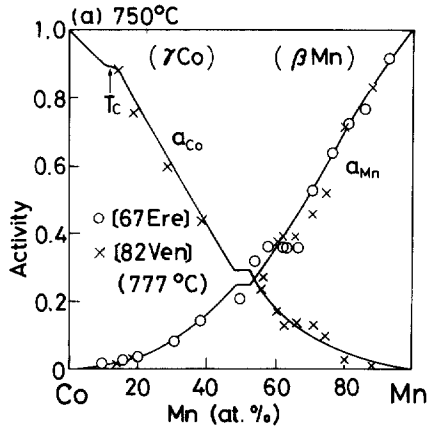

K. Ishida and T. Nishizawa, 1990.

Table 8 Lattice Stability Parameters of Co-Mn Solution Phases

From [78Kau]

$G^0(Co,P) - G^0(Co,K) = -3347 + 1.841\,T\,(T > 300\ K)$

$G^0(Co,fcc) - G^0(Co,P) = -4443 - 9.045\,T + 1.7218 \times 10^{-2}T^2 - 0.67509 \times 10^{-5}T^3\,(T > 300\ K)$

$G^0(Co,bcc) - G^0(Co,fcc) = 6953 - 0.63137 \times 10^{-2}T^2 + 2.8037 \times 10^{-6}T^3\,(T < 1800\ K)$

$G^0(Co,L) - G^0(Co,bcc) = 13\,849 - 19.163\,T$

$G^0(Co,L) - G^0(Co,cph) = 16\,652.3 - 9.7906\,T$

$G^0(Mn,P) - G^0(Mn,K) = 2259.4 - 2.259\,T\,(T < 1220\ K)$

$G^0(Mn,fcc) - G^0(Mn,P) = 611 + 13.101\,T - 2.124 \times 10^{-2}T^2 - 0.8396 \times 10^{-5}T^3\,(400 < T < 1220\ K)$

$G^0(Mn,bcc) - G^0(Mn,fcc) = -1477 + 0.514\,T + 2.742 \times 10^{-3}T^2 - 1.6534 \times 10^{-6}T^3\,(400 < T < 1220\ K)$

$G^0(Mn,L) - G^0(Mn,bcc) = 14\,644 - 9.623\,T\,(T < 1220\ K)$

$G^0(Mn,L) - G^0(Mn,cph) = 9205 - 7.113\,T\,(T < 1220\ K)$

From [82Has]

$G^0(Co,fcc) - G^0(Co,P) = -510 - 1.56\,T(a)$

$G^0(Co,bcc) - G^0(Co,fcc) = 7714 - 3.629\,T(a)$

$G^0(Co,L) - G^0(Co,bcc) = 8476 - 5.534\,T(a)$

$G^0(Co,L) - G^0(Co,cph) = 16\,640 - 9.807\,T(a)$

$G^0(Mn,fcc) - G^0(Mn,P) = 2200 - 1.618\,T$

$G^0(Mn,bcc) - G^0(Mn,fcc) = 1800 - 1.276\,T(a)$

$G^0(Mn,L) - G^0(Mn,bcc) = 14\,650 - 9.655\,T$

From [83Cha]

$G^0(Mn,P) - G^0(Mn,K) = 2230 - 2.292\,T$

$G^0(Mn,fcc) - G^0(Mn,P) = 2120 - 1.561\,T$

$G^0(Mn,bcc) - G^0(Mn,fcc) = 1880 - 1.335\,T$

$G^0(Mn,L) - G^0(Mn,bcc) = 12\,060 - 7.939\,T$

Note: Values in J/mol; T in K. L: liquid, P: primitive cubic-βMn, K: complex cubic-αMn. **(a)** Paramagnetic term.

Fig. 8 Calculated Activities of Mn and Co at 1570 °C with Experimental Data

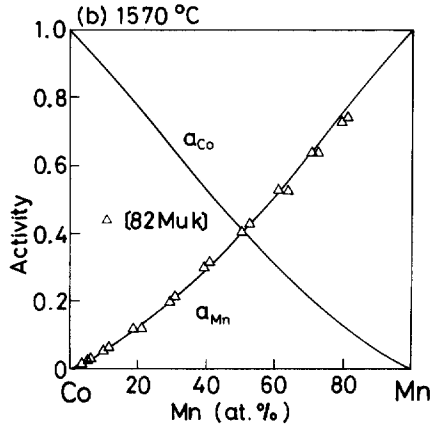

K. Ishida and T. Nishizawa, 1990.

Table 9 Co-Mn Interaction Parameters

Component	Interaction parameters, J/mol From [78Kau]	From [82Has](a)
K	$-17\,552 - 2.385\,T$	...
P	$-23\,849 - 2.385\,T$	$-43\,100 + 15.73\,T$
fcc	$-23\,849$	$-44\,860 + 20.39\,T$
bcc	$-26\,150$	$-45\,320 + 19.33\,T$
cph	$-28\,660 + 2.510\,T$	...
L	$-30\,962$	$-58\,250 + 25.09\,T + (-4620 + 1.75\,T)(X_{Mn} - X_{Co})$

Note: T in K. **(a)**Paramagnetic term.

Table 10 Magnetic Properties of Co-Mn Alloys

Phase	Composition, at.% Mn	Magnetic critical temperature, °C Curie	Néel	Paramagnetic → superantiferromagnetic	Magnetic moment, μ_B
From [32Has]					
(αCo)	5.27	986	...	...	...
From [37Has]					
(αCo)	5.3	995	...	...	...
	10.7	831	...	...	...
	15.9	657	...	...	...
From [56Kas]					
(αMn)	100	...	−178	...	(a)
From [57Cra]					
(αCo)	2.0	1077	...	...	1.693
	3.83	1022	...	...	1.648
	5.25	970	...	...	1.593
	10.50	827	...	...	1.362
	18.52	563	...	...	0.983
(εCo)	2.0	...	...	...	1.627
	3.83	...	...	...	1.556
	5.25	...	...	...	1.457
	10.50	...	...	...	1.240
	18.52	...	...	...	0.92(b)
From [58Wei]					
(αMn)	100	...	−178	...	(a)
(γMn)	100	...	307	...	2.3
(δMn)	100	...	354?	...	~1
From [70Mas](c)					
(αCo)	5.0	973	...	...	...
	10.3	825	...	...	...
	13.4	736	...	...	...
	15.4	680	...	...	...
	17.5	626	...	...	...
	19.5	563	...	...	...
	20.4	530	...	...	...
	21.7	485	...	...	...
	23.5	405	...	...	...
	24.6	375	...	...	...
	25.1	330	...	...	...
	26.8	275	...	...	...
	27.7	218	...	...	...
	28.7	100	...	...	...
	29.6	0	...	...	...

(a)I, 1.54; II, 1.54; III, 1.54; IV, 0. **(b)** Presence of some (αCo) phase? **(c)**Data read from the figure. **(d)**I, 1.9; II, 1.7; III, 0.6; IV, 0.2.

(continued)

Table 10 Magnetic Properties of Co-Mn Alloys (continued)

Phase	Composition, at %Mn	Magnetic critical temperature, °C: Curie	Néel	Paramagnetic→ superantiferromagnetic	Magnetic moment, μ_B
From [70Mat](c)					
(Co)	5.3	873	...	...	1.34
	15.9	520	...	...	0.84
	24.3	235	...	...	0.60
	31.5	12	...	...	0.22
	36.6	−139	−258	...	0.02
	37.6	...	−230	...	...
	38.7	...	−218	...	...
From [70Yam]					
(αMn)	100	...	...	...	(g)
From [70Tsi](c)					
(αCo)	~24.7	~299	...	...	...
From [72Ada]					
(αCo)	48.0	...	70	...	0.6
From [76Wil](c)					
(αMn)	96.7	...	−118	...	...
	98.3	...	−141	...	...
	98.9	...	−152	...	...
From [85Men](c)					
(αCo)	10	827	...	...	...
	20	430	...	...	0.75
	25	237	...	...	0.30
	27	168	...	...	0.10
	29	−21	...	...	...
	32	...	...	−247	...
	34	...	...	−185	...
	36	...	...	−137	...
	38	...	...	−89	...
	39	...	...	−72	...
	40	...	...	−35	...
	41	...	...	−17	...
	42	...	...	2	...
	43	...	−113	19	...
	44	...	−49	35	...
	45	...	−17	53	...
	46	...	23	76	...
	50	...	81	140	...
	52	...	111	167	...
(εCo)	20	...	...	...	0.67
	25	...	...	...	0.33
	27	...	...	...	0.19
	29	...	...	...	0.01

(a)I, 1.54; II, 1.54; III, 1.54; IV, 0.**(b)**Presence of some (αCo) phase? **(c)**Data read from the figure.**(d)**I, 1.9; II, 1.7; III, 0.6; IV, 0.2.

ganese," *Proc. Phys. Soc., 68*, 830-832 (1955). (Thermo; Experimental)

56Kas: J.S. Kasper and B.W. Roberts, "Antiferromagnetic Structure of α-Manganese and a Magnetic Structure Study of β-Manganese," *Phys. Rev., 101*, 537-544 (1956). (Magnetism; Experimental)

57Cra: J. Crangle, "The Magnetization of Cobalt-Manganese and Cobalt-Chromium Alloys," *Philos. Mag., 2*, 659-668 (1957). (Magnetism; Experimental)

***57Hel:** A. Hellawell and W. Hume-Rothery, "The Constitution of Alloys of Iron and Manganese with Transition Elements of the First Long Period," *Philos. Trans. R. Soc. (London) A, 249*, 417-459 (1957). (Equi Diagram; Experimental; #)

57Tau: K.J. Tauer and R.J. Weiss, "An Analysis of the Specific Heat of α-Manganese and its Antiferromagnetic Structure," *J. Phys. Chem. Solids, 2*, 237-239 (1957). (Thermo, Magnetism; Theory)

58Wei: R.J. Weiss and K.J. Tauer, "Thermodynamics and Magnetic Structures of the Allotropic Modifications of Manganese," *J. Phys. Chem. Solids, 4*, 135-143 (1958). (Meta Phases, Thermo, Magnetism; Theory)

Fig. 9 Magnetic Phase Diagram for the Co-Mn System

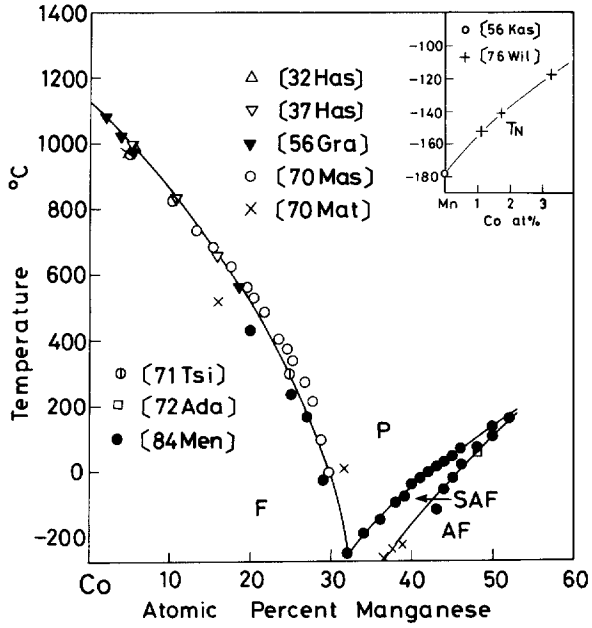

K. Ishida and T. Nishizawa, 1990.

67Ere: V.N. Eremenko, G.M. Lukashenko, and V.R. Sidorko, "Thermodynamic Properties of Manganese-Cobalt Solid Solutions," *Izv. Akad. Nauk SSSR, Met.*, (3), 192-196 (1967) in Russian; TR: *Russ. Metall.*, (3), 91-93 (1967). (Thermo; Experimental)

70Mas: H. Masumoto, S. Sawaya, and M. Kikuchi, "On the Thermal Expansion Coefficient, and Temperature Coefficient of Young's Modulus and its Equilibrium Diagram of Ferromagnetic Co-Mn Alloys," *Trans. Jpn. Inst. Met., 11*, 171-175 (1970). (Meta Phases, Magnetism; Experimental)

70Mat: M. Matsui, T. Ido, K. Sato, and K. Adachi, "Ferromagnetism and Antiferromagnetism in Co-Mn Alloy," *J. Phys. Soc. Jpn., 28*, 791 (1970). (Magnetism; Experimental)

70Yam: T. Yamada, N. Kunitomi, and Y. Nakai, "Magnetic Structure of α-Mn," *J. Phys. Soc. Jpn., 28*, 615-627 (1970). (Magnetism; Experimental)

71Sha: I.M. Sharshakov, V.S. Postnikov, D.E. Soldatenko, and L.V. Nikoforova, "Concerning the Phase Transformation in Co-Mn and Co-Cr Alloys," *Fiz. Met. Metalloved., 31*, 1114-1117 (1971) in Russian; TR: *Phys. Met. Metallogr., 31*, 231-234 (1971). (Meta Phases; Experimental)

***71Tsi:** K. Tsioplakis and T. Gödecke, "Supplement of the Cobalt-Manganese Phase Diagram," *Z. Metallkd., 62*, 680-681 (1971) in German. (Equi Diagram, Meta Phases, Magnetism; Experimental; #)

72Ada: K. Adachi, K. Sato, M. Matsui, and S. Mitani, "Magnetic Properties of fcc Co-Mn-Fe System," *IEEE Trans. Mag., 8*, 693-695 (1972). (Magnetism; Experimental)

72Wei: R.J. Weiss, "The Invar Effect," *Philos. Mag., 26*, 261-263 (1972). (Crys Structure; Theory)

73Ada: K. Adachi, K. Sato, M. Mitsui, and S. Mitani, "Neutron Diffraction Investigation of $(CoMn)_{1-x}Fe_x$," *J. Phys. Soc. Jpn.*, 35, 426-433 (1973). (Magnetism; Experimental)

73Kau: L. Kaufman and H. Nesor, "Calculation of the Binary Phase Diagrams of Iron, Chromium, Nickel and Cobalt," *Z. Metallkd.*, 249-257 (1973). (Thermo; Theory)

75Gud: V.N. Gudzenko and A.F. Polesya, "Metastable Phases in Mn-Base Alloys," *Izv. Akad. Nauk SSSR, Met.*, (5), 192-195 (1975) in Russian. TR: *Russ. Met.*, (5), 153-156 (1975). (Meta Phases, Crys Structure; Experimental)

76Wil: W. Williams and J.L. Stanford, "Antiferromagnetism of the α-Mn System," *J. Magn. Magn. Mater., 1*, 271-285 (1976). (Magnetism; Experimental)

78Kau: L. Kaufman, "Coupled Phase Diagrams and Thermodynamical Data for Transition Metal Binary System - III," *Calphad, 2*, 117-146 (1978). (Thermo; Theory; #)

79Ben: W. Bendick and W. Pepperhoff, "Thermally Excited States in Cobalt and Cobalt Alloys," *J. Phys. F, 9*, 2185-2194 (1979). (Thermo; Experimental)

80Gre: I.P. Gregory and D.E. Moody, "Low Temperature Specific Heat and Magnetization of Some Cobalt Based Alloys," *J. Magn. Magn. Mater., 15-18*, 281-282 (1980). (Thermo; Experimental)

80Rhi: D.R. Rhiger, D. Müller and P.A. Beck, "Micromagnetism in FCC Co-Mn Alloys," *J. Magn. Magn. Mater., 15-18*, 165-166 (1980). (Magnetism; Experimental)

81Ind1: G. Inden, "The Role of Magnetism in the Calculation of Phase Diagrams," *Physica, 103B*, 82-100 (1981). (Thermo; Theory)

81Ind2: G. Inden, Presented at CALPHAD X, quoted in "Summary of Proceedings of the Tenth CALPHAD," *Calphad, 5*, 152 (1981). (Equi Diagram; Experimental)

***82Has:** M. Hasebe, K. Oikawa, and T. Nishizawa, "Computer Calculation of Phase Diagrams of Co-Cr and Co-Mn Systems," *J. Jpn. Inst. Met., 46*, 577-583 (1982) in Japanese. (Equi Diagram, Thermo; Experimental; #)

82Jac: K.T. Jacob and M. Iwase, "Three Phase Equilibria for Activity Determinations: System Co-Mn," *Z. Metallkd., 73*, 316-320 (1982). (Thermo; Experimental)

82Muk: K. Mukai, K. Funatsu, K. Wasai, and T. Kitajima, "Measurements of Activities of Manganese in Liquid Co-Mn Alloys by an Isobaric Method," *J. Jpn. Inst. Met., 46*, 863-869 (1982) in Japanese. (Thermo; Experimental)

82Ven: M. Venkataraman and J.P. Hajra, "Thermodynamics of Cobalt-Manganese Alloys Using Fluoride and Oxide Electrolytes," *Scr. Metall., 16*, 1043-1048 (1982). (Thermo; Experimental)

83Cha: M.W. Chase, "Heats of Transition of the Elements," *Bull. Alloy Phase Diagrams, 4*(1), 124 (1983). (Thermo; Compilation)

83Nis1: T. Nishizawa and K. Ishida, "The Co (Cobalt) System," *Bull. Alloy Phase Diagrams, 4*(4), 387-390 (1983). (Equi Diagram, Meta Phases, Crys Structure; Compilation)

83Nis2: T. Nishizawa, S.M. Hao, M. Hasebe, and K. Ishida, "Thermodynamic Analysis of Miscibility Gap Due to Order-

ing in Ternary Systems," *Acta Metall., 31*, 1403-1416 (1983). (Thermo; Theory)

85Men: A.Z. Menshikov, G.A. Takzei, Y.A. Dorofeev, V.A. Kazantsev, A.K. Kostyshin, and I.I. Sych, "The Magnetic Phase Diagram of Cobalt-Manganese Alloys," *Zh. Eksp. Teor. Fiz., 89*, 1269-1279 (1985) in Russian; TR: *Sov. Phys. JETP, 62*, 734-740 (1985). (Magnetism; Experimental)

86Hil: M. Hillert, "The Thermodynamic Properties of Manganese," *TRITA-MAC-0305* (1986). (Thermo; Theory)

87Gul: A.F. Guillermet, "Critical Evaluation of the Thermodynamic Properties of Cobalt," *Int. J. Thermophys., 8*, 481-510 (1987). (Thermo; Theory)

*Indicates key paper.

#Indicates presence of a phase diagram.

Co-Mn evaluation contributed by **K. Ishida** and **T. Nishizawa,** Departments of Metallurgy, Materials Science and Metal Processing, Faculty of Engineering, Tôhoku University, Sendai 980, Japan. Work was supported by the Japanese Committee for Alloy Phase Diagrams. Part of the literature search was provided by ASM INTERNATIONAL. Literature searched through 1987. Professor Nishizawa is the ASM/NIST Category Editor for binary cobalt alloys.

The Co-In (Cobalt-Indium) System

By H. Okamoto
ASM INTERNATIONAL

Equilibrium Diagram

Because there are few experimental phase boundary data, the assessed Co-In phase diagram (Fig. 1) depends on a thermodynamic model proposed by [79Pre], which is based on thermal (data shown in Fig. 1), metallographic, and X-ray analyses of [70Sch]. Special points of Fig. 1 are listed in Table 1. The assessed diagram is quite different from that of [54Khl], who examined eight alloys metallographically (see [Elliott] or [Massalski]). The characteristics of the assessed diagram include liquid immiscibility, whereas the diagram of [54Khl] showed congruently melting "Co_3In_2" together with CoIn, and $CoIn_2$.

(Co) Terminal Phases

The melting point of αCo and the αCo ↔ εCo allotropic transformation temperature are 1495 and 422 °C, respectively [83Nis]. No solubility of In in (Co) was detected from the change of Curie and transition temperatures of (Co) [52Kos].

L_1 ↔ (αCo) + L_2 Monotectic Reaction

The existence of liquid immiscibility was reported by [68Das], and the monotectic temperature was determined to be 1286 °C by [70Sch]. The compositions of the two liquids at this temperature were estimated to be 23 and 75 at.% In [70Sch]. The symmetric shape of the assessed miscibility gap is based on a regular-solution model of [79Pre] (see "Thermodynamics" section). The calculated critical temperature of the miscibility gap is 1455 °C, which appears to be a reasonable estimate.

$CoIn_2$

The peritectic formation temperature of $CoIn_2$ is 550 ± 4 °C [70Sch]. The liquidus composition at this temperature is 99.6 at.% In according to the thermodynamic model of [79Pre], or ~92 at.% In, as conjectured by [70Sch]. Both values are tentative.

$CoIn_3$

The peritectic formation temperature of $CoIn_3$ is 490 ± 4 °C [70Sch].

(In) Terminal Phase

The melting point of In is 156.634 °C [Melt]. The solubility of Co in (In) is unknown.

Other Phases

[54Khl] found three compounds (Co_3In_2, CoIn, and $CoIn_2$) in alloys prepared at 200 to 250 °C and proposed

Table 1 Special Points of the Assessed Co-In Phase Diagram

Reaction	Compositions of the respective phases, at.% In			Temperature, °C	Reaction type
L_1 ↔ αCo		0		1495	Melting point
αCo ↔ εCo		0		422	Allotropic
L ↔ L_1 + L_2		~50		~1455	Critical point
L_1 ↔ (αCo) + L_2	23	0	~77	1286	Monotectic
(αCo) + L_2 ↔ $CoIn_2$	0	~99.6	66.7	550	Peritectic
$CoIn_2$ + L_2 ↔ $CoIn_3$	66.7	~99.7	75	490	Peritectic
L_2 ↔ $CoIn_3$ + (In)	~100	75	100	156	Eutectic
L_1 ↔ In		100		156.634	Melting point